Stability of vortex flow in a modulated channel

Ehab Abu-Ramadan and Roger E. Khayat*
Department of Mechanical and Materials Engineering, The University of Western Ontario, London, Ontario, Canada N6A 5B9
(Received 7 September 2005; revised manuscript received 15 November 2006; published 7 February 2007)

Linear stability analysis of a fully developed two-dimensional periodic steady flow in a spatially modulated symmetric channel is investigated numerically. Both walls are sinusoidally modulated. The modulation amplitude is assumed to be small. The base steady flow is calculated using a regular perturbation expansion of the flow field coupled to a variable-step finite-difference scheme. The disturbance flow equations are derived within the framework of Floquet theory and solved using a two-point boundary value method. The implemented procedure is simple, direct, and very efficient. The accuracy of this method is established. The influence of geometric parameters on the threshold for the onset of instability is systematically investigated. It is established that the critical Reynolds number for the onset of hydrodynamic instability decreases as the wall modulation amplitude or wave number increases. Modulated channel flow is characterized by the formation of a recirculation region or vortices beneath the modulation crest as the Reynolds number exceeds a certain critical threshold. The relation between the thresholds for the onset of instability and vortex flow is examined over a wide range of geometric parameters. Vortex flow effects on the conditions for the onset of instability are systematically investigated. The parameter regime of stable vortex flow is established. It is found that the parameter regime of stable vortex flow increases significantly with the wall modulation wave number for small wave numbers. This increase become less pronounced as the wave number is further increased.

DOI: 10.1103/PhysRevE.75.026305 PACS number(s): 47.20.−k, 47.11.−j, 47.15.Fe

I. INTRODUCTION

Flow inside corrugated passages is observed in various natural phenomena and industrial processes. In some cases, the wall corrugation is a natural artifact of a machining process, while in other applications, the modulation is incorporated into the design to modify the flow for the purpose of enhanced mixing or heat transfer as encountered in compact, high-flux heat exchangers, and membrane blood oxygenators [1,2]. Flow through modulated passages is of interest to physiologists because of its relation to blood and urinary flow [3,4]. Furthermore, the converging-diverging nature of the periodically modulated channels captures the quintessential features of porous media flow, as in the case of tertiary oil recovery, paper and textile coating, composite manufacturing, and biological transport processes [5–8]. In spite of the apparent geometrical simplicity, these flows can contain separated flow regions and exhibit many of the features present in much more complex geometries [9–11]. Wall corrugation is expected to affect the critical conditions for the onset of hydrodynamic instabilities. Influence of wall waviness on the transition from laminar to turbulent flow is of practical importance since it touches almost every field of fluid dynamics from biology to aeronautics [12]. This richness in physical phenomena in a relatively simple geometry is behind the ongoing fundamental interest.

Most of the earlier studies on the flow through wavy passages are mainly concentrated on the conditions under which steady vortex flow emerges [4,13–15]. The vortex flow, sometimes referred to as backflow, is a flow with wall-bound recirculation. It is typically predicted that vortex flow sets in once the Reynolds number exceeds a critical threshold Re_c which depends on the modulation shape. As Re increases above Re_c, the size of the vortex increases until the vortex spans the entire period of the modulation. Pressure-driven flow in smooth passages (*Poiseuille flow*) is expected to lose its stability at a critical Reynolds number in the form of standing or traveling Tollmien-Schlichting (TS) waves. The presence of surface waviness or roughness alters the conditions and the scenario for the laminar-turbulent transition. A number of experimental studies [16–20] have shown that even mild surface roughness can cause the appearance of two- and three-dimensional instabilities. These instabilities can, in turn, lead to laminar-turbulent transition at lower Reynolds number in comparison with Poiseuille flow. In other words, empirical observations show that a rough surface promotes transition to turbulent flow. The wall roughness effect is reminiscent of the influence of the induced small-amplitude surface acoustic wave along the walls of a parallel-plane channel on the stability of fully developed incompressible flow [21]. The stability of fully developed flows between two infinite porous plane walls with uniform injection at the lower wall and suction at the upper wall is characterized by a critical injection rate, above which higher injection rates are found to stabilize the flow [22].

The question as to whether flow through wavy passages loses its stability prior to the onset of vortex flow is still relatively unexplored. Hence, it is the main focus of the present study. A linear stability analysis was carried out by Selvarajan *et al.* [3] and Cabal *et al.* [12] for the flow through weakly modulated channels, i.e., small wall modulation amplitude. They showed that wall waviness promotes hydrodynamic instability, and the flow loses its stability prior to the onset of vortex flow for the examined range of geometric parameters. Nishimura *et al.* [23,24] carried out a flow visualization study for strongly sinusoidally modulated channel flow. They observed that the flow remains steady,

*Author to whom correspondence should be addressed. Email address: rkhayat@eng.uwo.ca

with streamlines parallel to channel walls, until Re reaches the critical value $Re_c=15$, at which stage steady vortex flow emerges. The steady vortex flow loses its stability to two-dimensional oscillatory vortex flow at a Reynolds number approximately equal to 100. There did not seem to be any breakdown of the two-dimensional roll into a three-dimensional vortex. Using the same geometry, Blancher *et al.* [25] confirmed Nishimura *et al.*'s results by applying linear stability analysis of the fully developed vortex flow, and found that oscillatory vortex flow sets in at a Reynolds number approximately equal to 90. A direct transient three-dimensional numerical simulation by Guzman and Amon [26], using a spectral-element method, confirmed the findings of both Blancher *et al.* [25] and Nishimura *et al.* [23,24]. Similar predictions were made by Lahbabi and Chang [27], who used a global Galerkin-spectral method to solve the fully three-dimensional transient Navier-Stokes equations in periodically constricted tubes. They found that while the critical Reynolds number for the onset of vortex flow is 51, the flow loses its stability via a Hopf bifurcation as the Reynolds number exceeds 200. These results are based on a tube characterized by a moderate modulation amplitude and large wave number. Flow separation was shown to occur even under creeping conditions if the modulation amplitude is strong enough [9,27].

The foregoing studies indicate that, depending on the geometric parameters, the flow loses its stability to a two-dimensional oscillatory flow either prior to or after the onset of vortex flow. However, Lahbabi and Chang [27] showed that, although the flow may be stable to two-dimensional or axisymmetric disturbances, it may be unstable to three-dimensional disturbances. A systematic study on the influence of geometric parameters on the onset of hydrodynamic instability is required to determine the regions of stable vortex flow. None of the previously reported studies examined the variation of the wall modulation amplitudes and wave numbers on the stability of vortex flow. While some investigators considered only a single geometric configuration [23–26], others examined the variation of the onset of instability threshold over limited range of modulation amplitudes [3,12]. The question as to how the appearance of vortex flow affects the conditions for the onset of instability is still relatively unexplored.

Since the flow in modulated channels is of fundamental and practical interest, it is desirable to systematically investigate the influence of the modulation wavelength and amplitude on hydrodynamic stability over a wide range of flow parameters. This is one of the objectives of the current study. The relation between the critical Re for the onset of hydrodynamic instability, Re_t, and the geometric parameters will be determined. Regions of stable vortex flow will be established upon the comparison between the critical conditions for the onset of instability and vortex flow for various combinations of geometric parameters. Vortex flow is stable if the corresponding Reynolds number is below the threshold for the onset of instability ($Re < Re_t$).

The stability analysis of viscous flow through wavy passages is a computationally demanding task since both streamwise and depthwise directions are spatially inhomogeneous, thereby ruling out closed form solutions for the base flow. The domain perturbation approach as described by Zhou *et al.* [13,14] is applied here to generate the steady state solution for the flow through modulated channels. Since the accuracy of this approach depends on the amplitude of the modulation, the present study will be limited to weakly modulated channels. The disturbance flow equations are derived within the framework of Floquet theory [28], and solved using a two-point boundary value method [29,30]. The two-point boundary value method can be described in two steps. First, the ordinary differential equations describing the disturbance flow are set as an equivalent first-order system of ordinary differential equations with conditions at two end points. Second, the resulting system is numerically solved using a two-point solver code [31]. Unlike spectral methods [32], the proposed method provides highly accurate solutions for high Reynolds number flow [30]. The numerical efficiency is further improved upon the implementation of the primitive variables, viz. velocity and pressure, instead of the stream function.

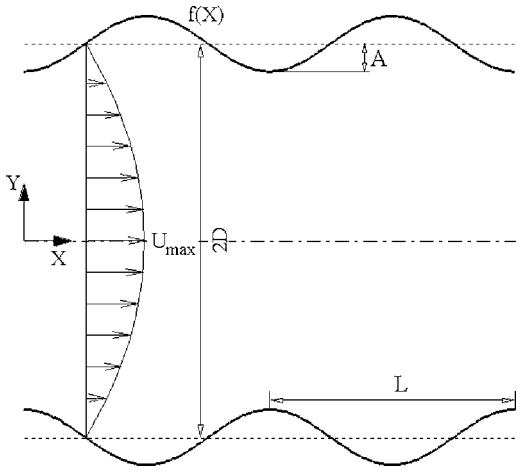

FIG. 1. Physical domain and flow configuration for spatially modulated channel.

II. PROBLEM FORMULATION AND SOLUTION PROCEDURE

In this section, the general equations and boundary conditions for the pressure-driven flow between spatially modulated walls are introduced. A regular perturbation expansion of the flow field coupled to a variable-step finite-difference scheme is used to determine the base flow. The disturbance equations are derived within the framework of Floquet theory, and solved using a two-point boundary value method.

A. Governing equations

Consider the flow of an unsteady, incompressible Newtonian fluid of density ρ and viscosity μ. The flow is pressure driven between two infinite rigid wavy walls as shown in Fig. 1. Both walls have the same wavelength L and are assumed infinite in extent in the streamwise X and spanwise Z directions. The general shapes of the bottom and top boundaries are given by $Y_B(X)=-D-Af(X)$ and $Y_T(X)=D+Af(X)$,

respectively, where A is the modulation amplitude, and D is the average half gap width. Here $f(X)$ is a general function of X that may be arbitrarily prescribed. In this work, however, only sinusoidal modulation will be considered. More complex geometries can be described by a general Fourier series as illustrated by Zhou *et al.* [14].

Let D, $U_{\max}$, and $D/U_{\max}$ be the characteristic length, velocity, and time, respectively. In this case, $U_{\max}$ is the maximum velocity for Poiseuille flow between two flat plates, with the upper and lower plates coinciding with the mean height of the modulated walls. The pressure is normalized by $\mu U_{\max}/D$. After the dimensionless variables are introduced, four dimensionless groups emerge in the problem, namely, the Reynolds number Re, the aspect ratio ε, the dimensionless wavelength λ, and the wall modulation wave number α:

$$\mathrm{Re} = \frac{\rho U_{\max} D}{\mu}, \quad \varepsilon = \frac{A}{D}, \quad \lambda = \frac{L}{D} = \frac{2\pi}{\alpha}. \tag{1}$$

The dimensionless conservation equations for mass and momentum are

$$\nabla \cdot \mathbf{u} = 0, \tag{2a}$$

$$\mathrm{Re}(\partial \mathbf{u}/\partial t + \mathbf{u} \cdot \nabla \mathbf{u}) = -\nabla p + \nabla^2 \mathbf{u}, \tag{2b}$$

where $\mathbf{u}(u,v)$ is the velocity vector and p is the pressure. The above equations must be solved subject to the no-slip and no-penetration boundary conditions, such that

$$\mathbf{u}(x, y = \pm h(x), t) = 0, \tag{3a}$$

and the condition of periodicity

$$\mathbf{u}(x,y,t) = \mathbf{u}(x+\lambda, y, t), \tag{3b}$$

$$p(x,y,t) = p(x+\lambda, y, t) - \lambda \Delta p, \tag{3c}$$

where $h(x) = 1 + \varepsilon f(x)$ is the distance between the centerline and the wall and Δp is the linear pressure drop per unit length. The assumption that the fully developed flow has the same periodic length as the wall modulation has been verified both experimentally and numerically by numerous investigators [5,23,33].

The flow variables are expressed as a superposition of the steady flow $(\bar{u}, \bar{v}, \bar{p})$ and the infinitesimal unsteady two-dimensional disturbances $(\tilde{u}, \tilde{v}, \tilde{p})$ such that

$$u(x,y,t) = \bar{u}(x,y) + \tilde{u}(x,y,t), \tag{4a}$$

$$v(x,y,t) = \bar{v}(x,y) + \tilde{v}(x,y,t), \tag{4b}$$

$$p(x,y,t) = \bar{p}(x,y) + \tilde{p}(x,y,t). \tag{4c}$$

The steady flow $(\bar{u}, \bar{v}, \bar{p})$ is obtained using the domain perturbation approach coupled to a variable-step finite-difference scheme as adopted by Zhou *et al.* [13,14]. The solution is, therefore, limited to small modulation ($\varepsilon < 0.3$ and $\alpha < 2$) [14]. The small-disturbance solution is sought next.

B. The disturbance flow

Substituting expression (4) into Eqs. (2), and neglecting quadratic terms in the disturbance flow components, we obtain

$$\tilde{u}_x + \tilde{v}_y + \tilde{w}_z = 0, \tag{5a}$$

$$\mathrm{Re}(\tilde{u}_t + \bar{u}\tilde{u}_x + \tilde{u}\bar{u}_x + \bar{v}\tilde{u}_y + \tilde{v}\bar{u}_y) = \tilde{u}_{xx} + \tilde{u}_{yy} - \tilde{p}_x, \tag{5b}$$

$$\mathrm{Re}(\tilde{v}_t + \bar{u}\tilde{v}_x + \tilde{u}\bar{v}_x + \bar{v}\tilde{v}_y + \tilde{v}\bar{v}_y) = \tilde{v}_{xx} + \tilde{v}_{yy} - \tilde{p}_y, \tag{5c}$$

where a subscript denotes partial differentiation. The disturbance variables in Eq. (5) must be solved subject to the no-slip and no-penetration boundary conditions

$$\tilde{u}(x, y = \pm h(x), t) = \tilde{v}(x, y = \pm h(x), t) = 0, \tag{6a}$$

and the condition of periodicity

$$\tilde{\phi}(x = 0, y, t) = \tilde{\phi}(x = \lambda, y, t), \tag{6b}$$

where $\tilde{\phi}$ represents $\tilde{u}$, $\tilde{v}$, or $\tilde{p}$.

In order to overcome the difficulties associated with the presence of irregular boundaries, the periodic physical domain $\Omega_{xyt} = \{(x,y,t) \,|\, x \in [0,\lambda], y \in [0, 1+\varepsilon f(x)], t\}$ is mapped onto the rectangular computational domain $\Omega_{\xi\eta t} = \{(\xi,\eta,t) \,|\, \xi \in [0,\lambda], \eta \in [0,1], t\}$. In this case,

$$\xi(x,y,t) = x, \quad \eta(x,y,t) = \frac{y}{h(x)}. \tag{7}$$

Now the transformed equations read

$$\tilde{u}_\xi - \frac{\eta h'}{h}\tilde{u}_\eta + \frac{1}{h}\tilde{v}_\eta = 0, \tag{8a}$$

$$\mathrm{Re}\left[\tilde{u}_t + \tilde{u}\left(\bar{u}_\xi - \frac{\eta h'}{h}\bar{u}_\eta\right) + \bar{u}\left(\tilde{u}_\xi - \frac{\eta h'}{h}\tilde{u}_\eta\right) + \frac{\tilde{v}\bar{u}_\eta}{h} + \frac{\bar{v}\tilde{u}_\eta}{h}\right] = -\tilde{p}_\xi + \frac{\eta h'}{h}\tilde{p}_\eta + \tilde{u}_{\xi\xi} - \eta\left[\left(\frac{h''}{h} - 2\left(\frac{h'}{h}\right)^2\right)\tilde{u}_\eta + 2\frac{h'}{h}\tilde{u}_{\eta\xi}\right] + [1 + (\eta h')^2]\frac{\tilde{u}_{\eta\eta}}{h^2}, \tag{8b}$$

$$\mathrm{Re}\left[\tilde{v}_t + \tilde{u}\left(\bar{v}_\xi - \frac{\eta h'}{h}\bar{v}_\eta\right) + \bar{u}\left(\tilde{v}_\xi - \frac{\eta h'}{h}\tilde{v}_\eta\right) + \frac{\tilde{v}\bar{v}_\eta}{h} + \frac{\bar{v}\tilde{v}_\eta}{h}\right] = \frac{-\tilde{p}_\eta}{h} + \tilde{v}_{\xi\xi} - \eta\left[\left(\frac{h''}{h} - 2\left(\frac{h'}{h}\right)^2\right)\tilde{v}_\eta + 2\frac{h'}{h}\tilde{v}_{\eta\xi}\right] + [1 + (\eta h')^2]\frac{\tilde{v}_{\eta\eta}}{h^2}, \tag{8c}$$

where a prime denotes differentiation with respect to x. The boundary conditions for the disturbance flow become

$$\tilde{u}(\xi, \eta = \pm 1, t) = \tilde{v}(\xi, \eta = \pm 1, t) = 0, \tag{9a}$$

$$\tilde{\phi}(\xi = 0, \eta, t) = \tilde{\phi}(\xi = \lambda, \eta, t). \tag{9b}$$

Since the base flow (*steady flow*) is two dimensional only,

separation of variables is permissible, and the representation of the t dependence of the solution is in the form

$$\tilde{\phi}(\xi,\eta,t) = \tilde{\phi}^d(\xi,\eta)e^{-i\delta t}, \tag{10}$$

where $\tilde{\phi}^d$ represents $\tilde{u}^d$, $\tilde{v}^d$, or $\tilde{p}^d$. The exponent δ is assumed to be complex, whose imaginary part δ_I describes the rate of growth of the disturbances, and its real part δ_r describes the frequency of the disturbances. While the disturbances are damped if $\delta_I<0$ and the base flow is stable, they are amplified if $\delta_I>0$ and instability sets in.

Since the base flow is periodic in ξ with periodicity λ, the disturbance flow variables, can be expressed using the Floquet theory [28] such that

$$\tilde{\phi}(\xi,\eta,t) = \sum_{n=-\infty}^{n=\infty} [\tilde{\phi}^{(n)}(\eta)]e^{i[(\beta+n\alpha)\xi-\delta t]}, \tag{11}$$

where $\tilde{\phi}^{(n)}$ represents any of the amplitude functions $\tilde{u}^{(n)}$, $\tilde{v}^{(n)}$, or $\tilde{p}^{(n)}$. The expression $(\beta+n\alpha)$ results from the superposition of the channel wave number α and the real Floquet exponent β. In temporal stability analysis, β is the disturbance wave number. The streamwise periodicity occurs only if β/α is rational.

Substitution of expression (11) into Eq. (8) and separation of Fourier components using the orthogonality property of the complex exponential function results in an infinite set of homogeneous ordinary differential equations governing $\tilde{u}^n$, $\tilde{v}^n$, and $\tilde{p}^n$, where the parentheses have been dropped for simplicity. Those equations are given in Appendix C of Ref. [37], and have to be solved subject to the following boundary conditions:

$$\tilde{u}^n(\xi,\eta=\pm 1) = \tilde{v}^n(\xi,\eta=\pm 1) = 0, \tag{12a}$$

$$\tilde{\phi}^n(\xi=0,\eta) = \tilde{\phi}^n\left(\xi=\frac{2\pi}{\alpha},\eta\right). \tag{12b}$$

The homogeneous system presented in Appendix C in [37] along with the homogenous boundary conditions given in (12) is far more complicated than the classical Orr-Sommerfeld stability problem, which can be obtained upon setting $\varepsilon=0$. Wall modulation dramatically alters the problem structure. Despite those difficulties, the solution can be sought using similar techniques that are used to solve for the classical Orr-Sommerfeld problem. The description of the solution procedure is important and will be addressed next.

C. Solution procedure

The solution to the infinite set of coupled ordinary differential equations in Appendix C in [37] with the homogenous boundary conditions (12) can be approximated by truncating the sum after a finite number N, and then solving the coupled homogeneous $3\times(2N+1)$ differential equations. In order to avoid the difficulties associated with the pseudospectral method, a two-point boundary value numerical method as described by Ache and Cores [30] is employed to solve the eigenvalue problem. First, the eigenvalue problem is transformed into an equivalent two-point boundary value first-order system of the form

$$\mathbf{Z}_\eta = A(\beta,\delta,Re,\alpha,\varepsilon,\eta,\bar{u},\bar{v},\bar{p})\mathbf{Z}, \tag{13a}$$

$$\delta_\eta = 0, \tag{13b}$$

with the boundary conditions

$$\overleftrightarrow{\mathbf{B}}\cdot\mathbf{Z}(\eta=1)=0, \quad \overleftrightarrow{\mathbf{C}}\cdot\mathbf{Z}(\eta=-1)=0, \tag{14a}$$

$$z_k(\eta=1)=1, \tag{14b}$$

where the subscript η donates differentiation with respect to η, and for some k, $1\leqslant k\leqslant 8N+4$. $\mathbf{Z}$ is a complex vector, $\mathbf{Z}=(Z_1,Z_2,\ldots,Z_M)$, and $M=8N+4$. Consequently, $\overleftrightarrow{\mathbf{B}}$ and $\overleftrightarrow{\mathbf{C}}$ are $M\times M$ matrices. The auxiliary boundary condition (14b) has to be selected carefully to avoid conflict with the physical boundary condition (14a), and to avoid any trivial solutions. Ache and Cores [30] selected the first derivative of the disturbance streamwise velocity in the classical Orr-Sommerfeld stability problem to be equal to 1 at the upper wall as the auxiliary boundary condition. Because of the similarity between the current problem and the classical Orr-Sommerfeld equations, the same auxiliary boundary condition is used.

The homogeneous set of ordinary differential equations (13) with the corresponding nonhomogeneous boundary conditions (14) constitutes a boundary value problem of the two-point type. It is solved numerically using a variable-step finite-difference scheme (IMSL-DBVPFD) with a tolerance equal to 10^{-6}. The base discretization is the trapezoidal rule over a nonuniform mesh. This mesh is chosen adaptively, to make the local error approximately the same size everywhere. Higher-order discretizations are obtained by deferred corrections and global error estimates are produced to control the computation.

Due to the nonlinearity of the examined system in Eqs. (13) and (14), a careful selection of the initial iterate is required. The nonlinearity arises in the transient term. The initial iterate has to be closely related to the examined problem, and satisfy the boundary conditions. We select an initial iterate that is closely related to the Orr-Sommerfeld equation as proposed by Grosch and Salwan [34] and Ache and Cores [30]. A detailed discussion of the iterative technique to locate the critical Re for the onset of instability, Re_t, and the corresponding disturbance wave number β_t is outlined in the Ph.D. thesis by Abu-Ramadan [37].

Despite the lengthy computational time, the two-point boundary value method is easier to implement, and is believed to be of high accuracy since it avoids the computation of spurious modes as encountered sometimes by the spectral method [30]. A similar successive iteration procedure is also required to locate Re_t and β_t if the spectral method is used. In fact, Selvarajan *et al.* [3] carried out a considerable number of computations in the β-Re domain to locate Re_t and β_t for only two geometric configurations. While α for both configurations was 0.2, the selected ε were 0.05 and 0.1. Discussion of the accuracy of the numerical technique will be presented next.

III. VALIDATION AND NUMERICAL ASSESSMENT

Upon setting the wall modulation amplitude ε to zero, the limiting case of the plane Poiseuille flow is recovered. This limit case serves to validate the present numerical algorithm. Upon comparison between the currently calculated marginal stability curve for plane Poiseuille flow and the corresponding curve earlier reported by Ache and Cores [30], it can be demonstrated that both algorithms produce essentially identical curves. Based on the current stability calculation, the critical Reynolds number for the onset of hydrodynamic instability, $\mathrm{Re}_t=5772.219$, and the corresponding disturbance flow wave number $\beta_t=1.020\,55$. These values are in excellent agreement with the classical critical values set by Orszag [32], who reported that $\mathrm{Re}_t=5772.22$ and $\beta_t=1.020\,56\pm0.000\,01$.

The variation of the critical conditions for the onset of hydrodynamic instability as functions of the wall modulation amplitude ε can be used to assess the minimum truncation level of the disturbance flow field presentation in Eq. (11). Figure 2 shows the changes in Re_t, Fig. 2(a), and the corresponding β_t, Fig. 2(b), with ε for $\alpha=1.0$ and various values of $N\in[1,3]$. Figure 2(a) demonstrates that Re_t decreases as the wall modulation amplitude is increased. While the calculations based on both $N=2$ and $N=3$ predict essentially identical Re_t values over the examined ε range, quantitative differences are observed upon comparison of the predictions corresponding to $N=2$ and $N=1$ for $\varepsilon>0.03$. The relative error between the predictions for Re_t based on $N=1$ and $N=2$ does not exceed 3%. The relative error between the predictions based on $N=1$ and other truncation levels increases simultaneously with ε. The effect of the truncation level on the variation of the disturbance wave number β_t with the geometric parameters is illustrated in Fig. 2(b). In general, β_t increases with ε until the imposed ε reaches a critical value $\varepsilon_{\max}$, at which β_t reaches its maximum, and is referred to as $\beta_{t\max}$. Above $\varepsilon_{\max}$, β_t decreases as ε is increased. The quantitative differences may be traced back to the difficulty in locating β_t iteratively from the neutral stability curve because of the observed weak minima (see Fig. 5.2 in [37]). Furthermore, the relative error does not exceed the order of ε, which is the same order as the perturbation approach. Wall modulation does not seem to affect the order of β_t. This not surprising given the fact that β corresponds to the real Floquet exponent in (11).

Since the most important parameter in the present study is Re_t, one has to select a truncation level above which Re_t is unaffected. Figure 2 shows that Re_t becomes independent of the truncation level beyond $N=2$. Thus, the minimum disturbance flow field truncation level has to be 2. All subsequent predictions of the instability threshold are made using a disturbance flow field truncation level $N=2$. It is worth mentioning that Selvarajan *et al.* [1] did not examine the influence of the truncation level. They assumed that a truncation level $N=1$ is enough for reliable predictions of the critical conditions for the onset of instability. Clearly, this is not the case and their calculations must be reassessed for $N=2$.

IV. RESULTS AND DISCUSSION

Pressure-driven flow inside modulated channels is characterized by the appearance of vortex flow in the region of expansion below the crest as the Reynolds number exceeds a critical threshold Re_c. Whether the steady flow loses its stability prior to the onset of vortex flow is an important question, and will be addressed. The stability of vortex flow is also examined.

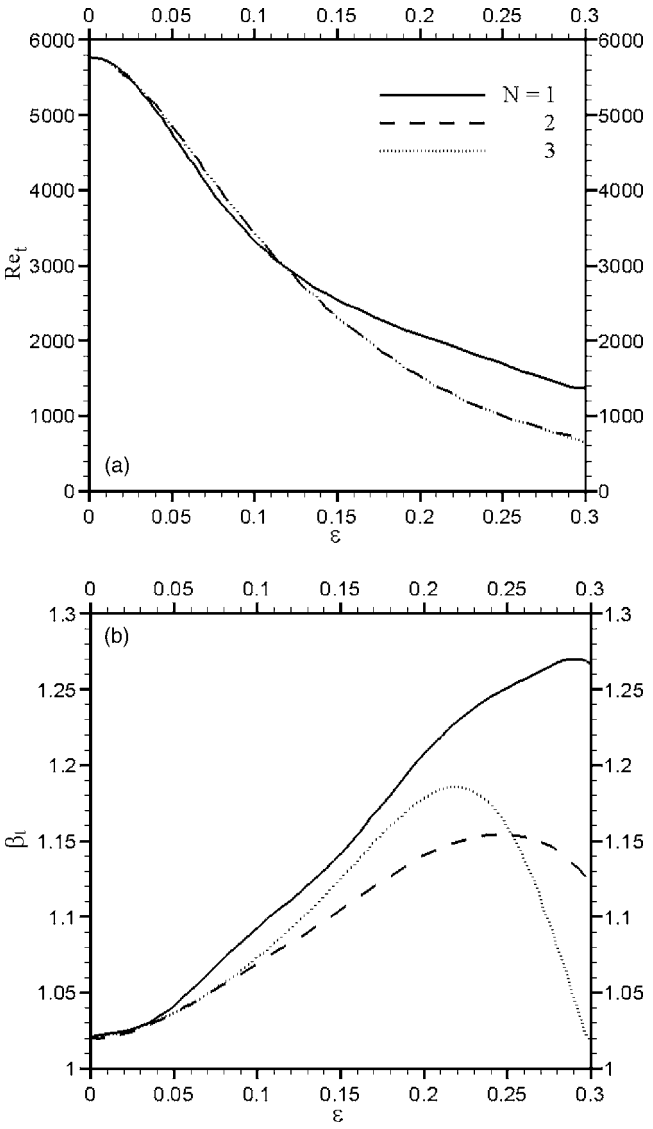

FIG. 2. Comparison between the influence of the truncation level N on the variation of the critical values, namely, Re_t (a) and β_t (b), with ε for $\alpha=1$. In both figures, solid, dashed, and dotted curves correspond to $N=1$, 2, and 3, respectively.

A. Influence of geometric parameters

An important threshold parameter for the current study is the critical Reynolds number for the onset of instability, Re_t. Figure 3 displays the variation of Re_t as a function of the wall modulation amplitude ε for various values of $\alpha\in[0.6,2]$. In general, Re_t decreases as both ε and α increase. This is in agreement with earlier results [16–20,35], which confirms that the presence of the wall corrugation precipitates the onset of instability. However, the relation between the geometric parameters and Re_t has not been previously

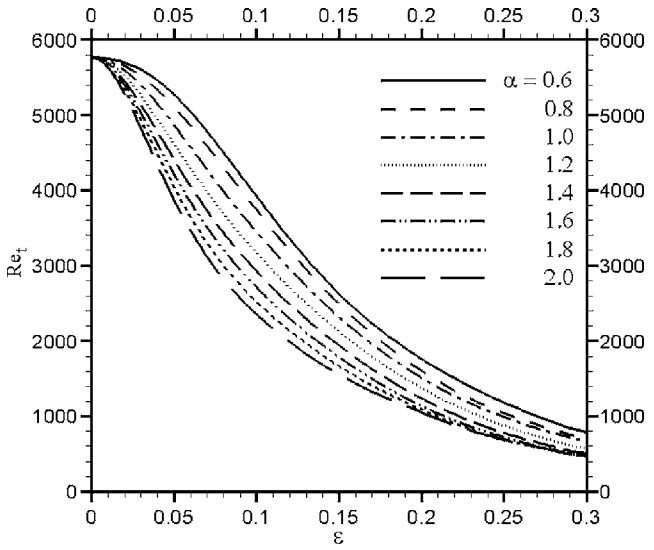

FIG. 3. Influence of the wall amplitude on the critical Re for the onset of instability, Re_t, for $\alpha \in [0.6, 2]$.

examined. This is simply because all earlier investigations considered only a single wave number over a small range of wall modulation amplitudes [3,12,23,25–27,33].

The present study reveals that, while a quadratic decrease is observed for $\varepsilon < 0.03$ and $\alpha < 1.2$, Re_t decreases exponentially when ε exceeds 0.03. The quadratic decrease in Re_t for $\varepsilon < 0.03$ confirms the earlier trend predicted by Cabal *et al.* [12] for $\varepsilon < 0.01$ and $\alpha = 1$. This is the only range reported by Cabal *et al.* [12]. Although Selvarajan *et al.* [3] attempted to investigate the relation between Re_t and ε for a larger range of wave amplitudes, $\varepsilon \in [0, 0.1]$, the reliability of their results is questionable because of the inadequate selection of the truncation level in their solution (see Sec. III). The relation between Re_t and α is examined by monitoring the changes in Re_t as α is increased for a constant ε. While Re_t decreases linearly as α is increased for $0.05 < \varepsilon < 0.15$, α does not seem to influence Re_t for $\varepsilon > 0.25$ and $\alpha \geqslant 1.6$. It is anticipated that geometric parameters would have a nonmonotonic influence on the onset of instability threshold. In the small-modulation limit $\varepsilon < 0.03$, geometric modulation may be neglected and the Poiseuille flow is essentially recovered. The critical Reynolds number for the onset of instability is thus expected to be close to the plane channel case, $\mathrm{Re} = 5772.219$. Stronger modulations are expected to alter the flow structure, and hence alter the critical conditions for the onset of instabilities. In particular, the rapid decrease of Re_t with increasing ε, which coincides with the onset of vortex flow, is similar to the exponential decrease in Re_c with ε [1,4,13,14]. Similar to the asymptotic decrease of Re_c toward the zero limit for a strongly modulated channel, Re_t seems to asymptotically decrease toward a critical value of order 100.

The effect of wall modulation is further investigated in Fig. 4, which shows the variation in the critical disturbance wave number β_t as a function of the wall modulation amplitude ε for $\alpha \in [0.6, 2.0]$. For a specified α, β_t increases with ε until ε reaches a critical value $\varepsilon_{\max}$, at which β_t reaches a maximum, $\beta_{t\,\max}$. There is also a change in concavity in the β_t curve that occurs at smaller ε as α increases. There is in

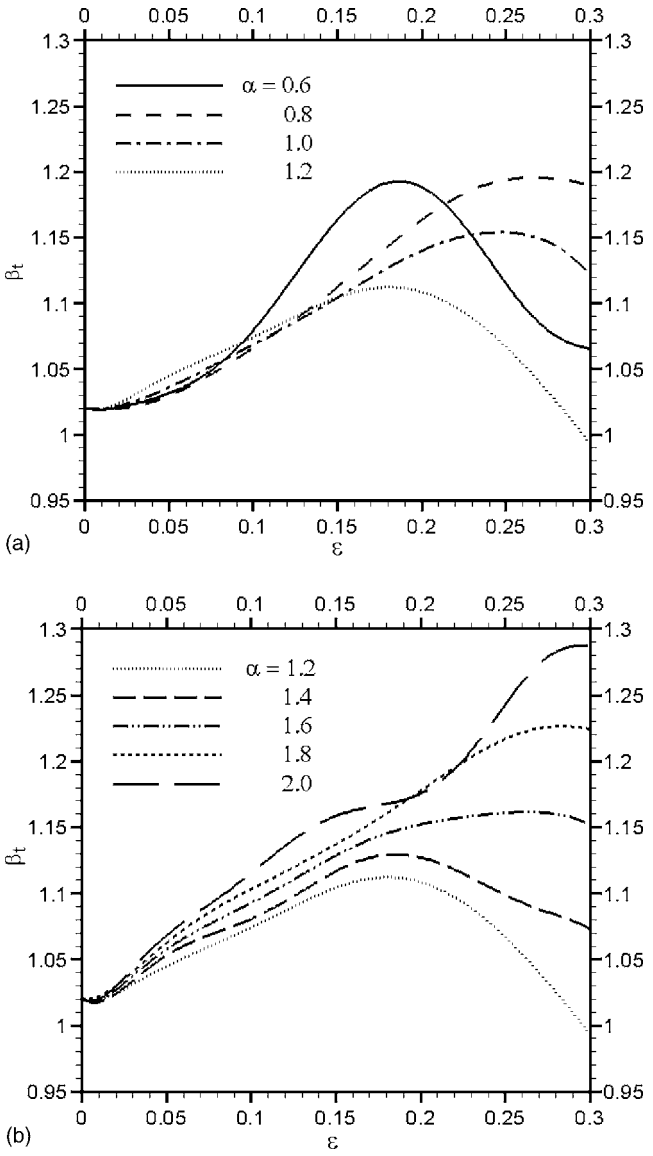

FIG. 4. Influence of the wall amplitude on β_t for $\alpha \in [0.6, 1.2]$ (top) and $\alpha \in [1.2, 2]$ (bottom).

fact a correlation between the change in concavity and onset of vortex flow (see below). In general, β_t appears to be larger than the wave number corresponding to nonmodulated (Poiseuille) flow, $\beta_{\mathrm{TS}} = 1.02$.

B. Stability of vortex flow

Steady-state calculations of the flow inside modulated channels reveal that recirculation regions or vortices form beneath the modulation crest beyond a certain critical Reynolds number Re_c. The size of the vortex flow regions changes as the Reynolds number is increased above Re_c. It is convenient to recall the influence of inertia on vortex formation. Figure 5 shows the changes in the streamline topology for the flow inside a modulated channel with $\varepsilon = 0.1$ and $\alpha = 1$ as function of inertia. In the absence of inertia, the streamlines are parallel to the channel wall profile, and the flow is symmetric with respect to the crest location. As iner-

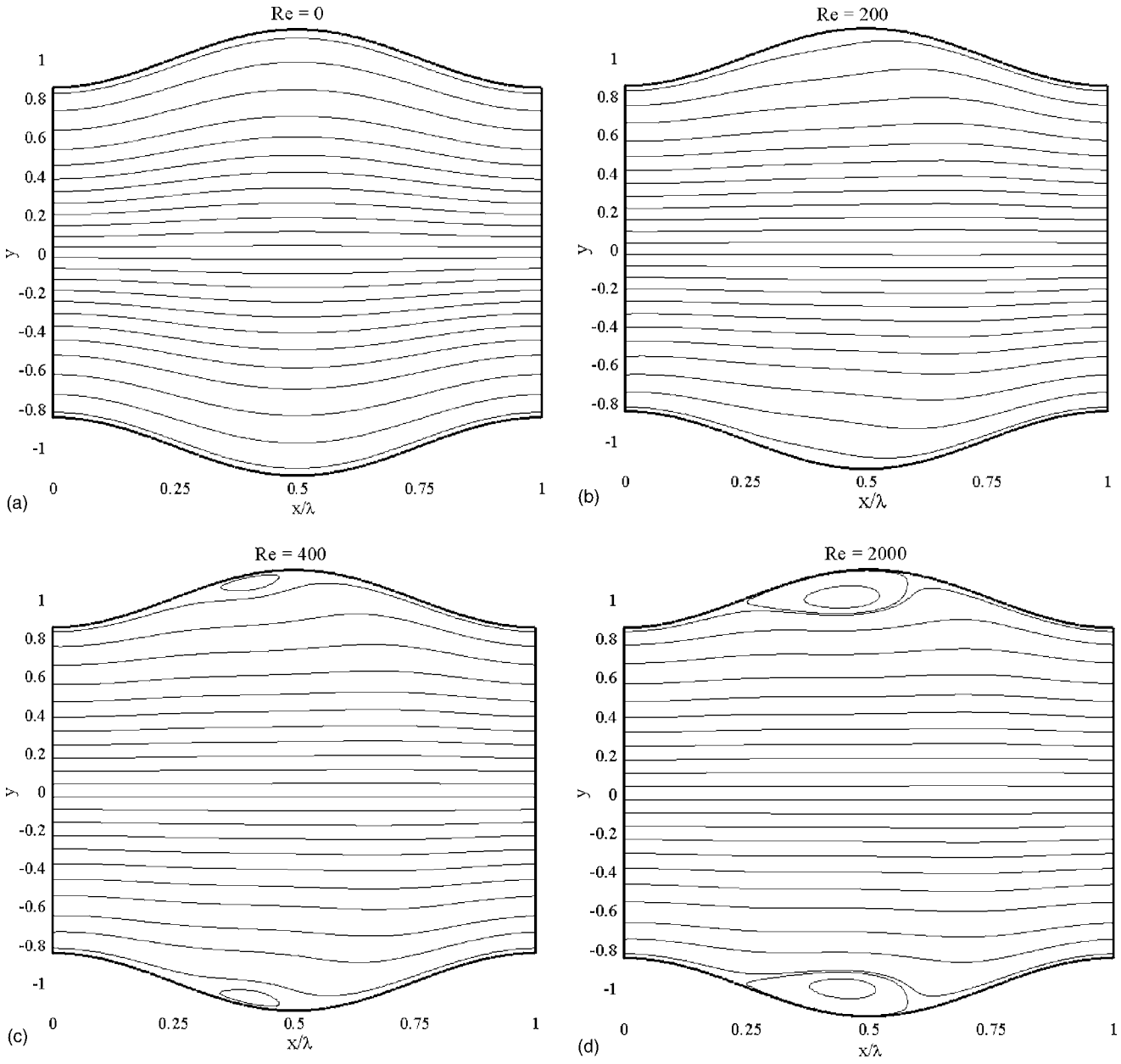

FIG. 5. Influence of Reynolds number on the steady-state flow streamlines for $\varepsilon=0.15$ and $\alpha=1$.

tia is introduced, the convective terms cause a break in symmetry, as illustrated for Re=200. The break in symmetry becomes more noticeable as inertia is further increased until Re exceeds Re_c, and flow separation (vortex flow) occurs in the region of expansion (below the crest). Figure 5 shows that at Re=400 a small recirculation vortex forms upstream of the wall crest. The flow reattaches immediately downstream of the crest. As Re is further increased, the size of the vortex increases, but eventually destabilizes. Flows at Re =200 and 400 illustrate the typical behavior in the pre- and postcritical ranges of Reynolds numbers, respectively. In the precritical range ($\mathrm{Re}<\mathrm{Re}_c$), prior to vortex formation, the flow is almost parallel to the wall modulation and will be referred to as *primary flow*. The flow in the postcritical range of Reynolds numbers ($\mathrm{Re}\geqslant\mathrm{Re}_c$) will be referred to as *vortex flow*. The steady-state flows reported in Fig. 5 are predicted to be linearly stable. In this case $\mathrm{Re}_t=3190$ (see Fig. 3).

The overall relation between vortex formation and flow stability is schematically illustrated in Fig. 6. The figure shows a schematic diagram of the dependence of Re_t and Re_c on ε, for given α. Different flow regions are identified. Region I represents stable primary flow, and region II (dashed region) represents stable vortex flow. Regions III and IV represent unstable primary flow and unstable vortex flow, respectively. Unlike the problems of Rayleigh-Benard (RB) convection and Taylor-Couette (TC) flow [36], there is no exchange of stability between the two distinct steady states. In fact, there is a unique steady state for modulated channel flow, and the steady flow structure changes gradually as the control parameter, say Re, increases. This figure assures the fact that the presence of recirculation is just a manifestation of inertial effects on base flow. Vortex flow should not be

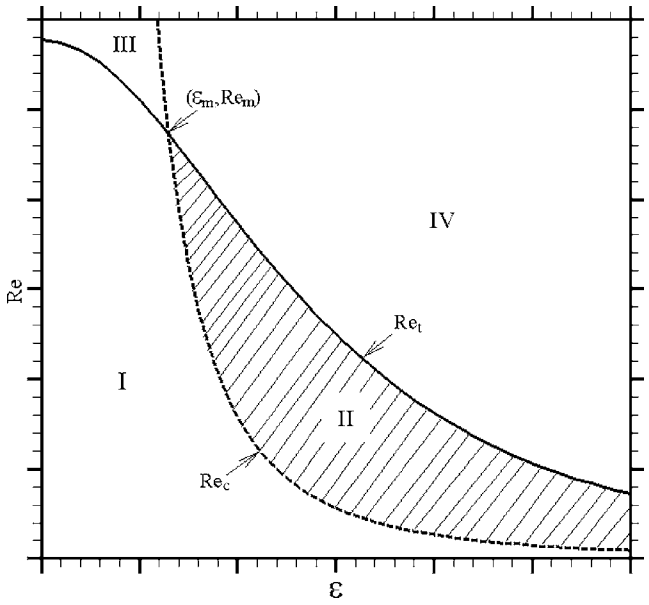

FIG. 6. Schematic comparison between the influence of the wall modulation amplitude on the critical Reynolds number for the onset of instability, Re_t, and the critical Reynolds number for the onset of vortex flow, Re_c. Regions of different dynamical behavior are denoted as I, stable primary flow; II, stable vortex flow; III, unstable primary flow; IV, unstable vortex flow.

viewed as instability. A range of parameters exist where steady vortex flow exists, as illustrated schematically in region II in this figure. In this region, $\mathrm{Re}_c < \mathrm{Re} < \mathrm{Re}_t$. The intersection between Re_t and Re_c indicates the minimum wall modulation amplitude ε_m required for the onset of stable vortex flow. This intersection also indicates the maximum Reynolds number Re_m above which no stable vortex flow sets in.

The influence of flow parameters can be further inferred from Fig. 7, which shows the dependence of Re_t and Re_c on ε for $\alpha \in [0.6, 2]$. The relation proposed by Zhou *et al.* [14] is implemented here to estimate Re_c, which is given by

$$\mathrm{Re}_c = 3.18\varepsilon^{-2.5}\alpha^{-2}. \tag{15}$$

Figure 7 shows that the size of the stable vortex flow region (region II) expands noticeably with α for $\alpha < 0.8$. As α is further increased above 0.8, the rate of increase in the stable vortex flow region becomes negligible. This dependence of the size of region II on the wall modulation wave number is expected given that Re_t decreases linearly with α and Re_c decreases as $1/\alpha^2$ [see Fig. 3 and Eq. (15)]. This dependence will be further explored upon examining the variations of Re_m and ε_m with α (see below). Figure 7 thus indicates that (stable) vortex flow is expected to be always observed at small Re for $\alpha > 0.8$ and $\varepsilon > 0.15$. The influence of the appearance of vortex flow on the conditions for the onset of instability can be inferred from the exponential decrease in Re_t with ε for $\varepsilon > \varepsilon_m$. Re_t decreases quadratically with increasing ε for $\varepsilon < \varepsilon_m$. Vortex flow thus promotes the onset of instability. Furthermore, comparison between Figs. 4 and 7 reveals that the change in concavity in the β_t vs ε curve occurs at essentially ε_m.

The relation between ε_m and α can be inferred from Fig. 8. This figure indicates that a functional relationship between ε_m and α exists, which is given by

$$\varepsilon_m = 0.05419\alpha^{-0.8161}. \tag{16}$$

The line in Fig. 8 shows the fit of this formula, and the symbols represent the values of the wall modulation amplitudes at the intersections of Re_t and Re_c in Fig. 7. The relationship of Eq. (16) can be used to estimate ε_m with a relative error $<1.5\%$ (see the inset in Fig. 8).

One has to be careful in interpreting the results in Fig. 8. It is well known that fits to data using special functions are notoriously poor for use in extrapolation. Along that line of reasoning, it might be improper to say, referring to (16), that there is an asymptotic decrease toward $\varepsilon_m \approx 0.02$. It is more appropriate to assume that there is an indication that stable vortex flow may not be observed for $\varepsilon < 0.02$. One cannot expect to see the asymptotic behavior as at $\alpha \to \infty$ from data fitted only through the range $0.6 < \alpha < 2.2$. In particular, Eq. (16) shows that the asymptote is zero, which is not true given the fact that flow inside modulated channels with relatively large α is expected to be similar to plane channel flow.

The relation between Re_m and α is illustrated in Fig. 9. A simple functional relation between Re_m and α could not be obtained. The solid line in Fig. 9 shows the fitting of the symbols representing the Reynolds numbers at the intersections of Re_t and Re_c in Fig. 7 using an eighth-order polynomial expansion. The inset shows the relative error resulting from the fitting. The variation of Re_m with α is complex but not surprising given the relations between Re_t and α in Fig. 3, and Re_c and α as established through Eq. (15). Figures 8 and 9 indicate that stable vortex flow cannot be observed for small wall modulation wave number ($\alpha < 0.5$) or small modulation amplitude ($\varepsilon < 0.02$). In this region, the flow loses its stability prior to the onset of vortex flow. Earlier studies by Selvarajan *et al.* [3] and Cabal *et al.* [12] were limited to $\varepsilon < 0.02$ or $\alpha = 0.2$. Thus, it is not surprising that neither of those two studies [3,12] managed to report stable vortex flow. Because of the abrupt increase in Re_m, accompanied by the significant decrease in ε_m for $\alpha < 0.8$, the stable vortex flow region expands noticeably as α increases within the range $0.2 < \alpha < 0.8$. A practical relation between Re_m and α may be obtained upon substituting expression (16) into Eq. (15), giving

$$\mathrm{Re}_m = 4651.33\alpha^{0.04029}. \tag{17}$$

Expression (17) can be used to estimate Re_m with a relative error below 4%.

V. CONCLUDING REMARKS

Linear stability analysis of a pressure-driven flow in a diverging-converging channel whose walls are described by simple sinusoidal functions has been explored using a two-point boundary value method over a wide range of geometric and flow parameters. The main advantages of the two-point boundary value numerical technique are its simplicity and high accuracy in comparison with other conventional meth-

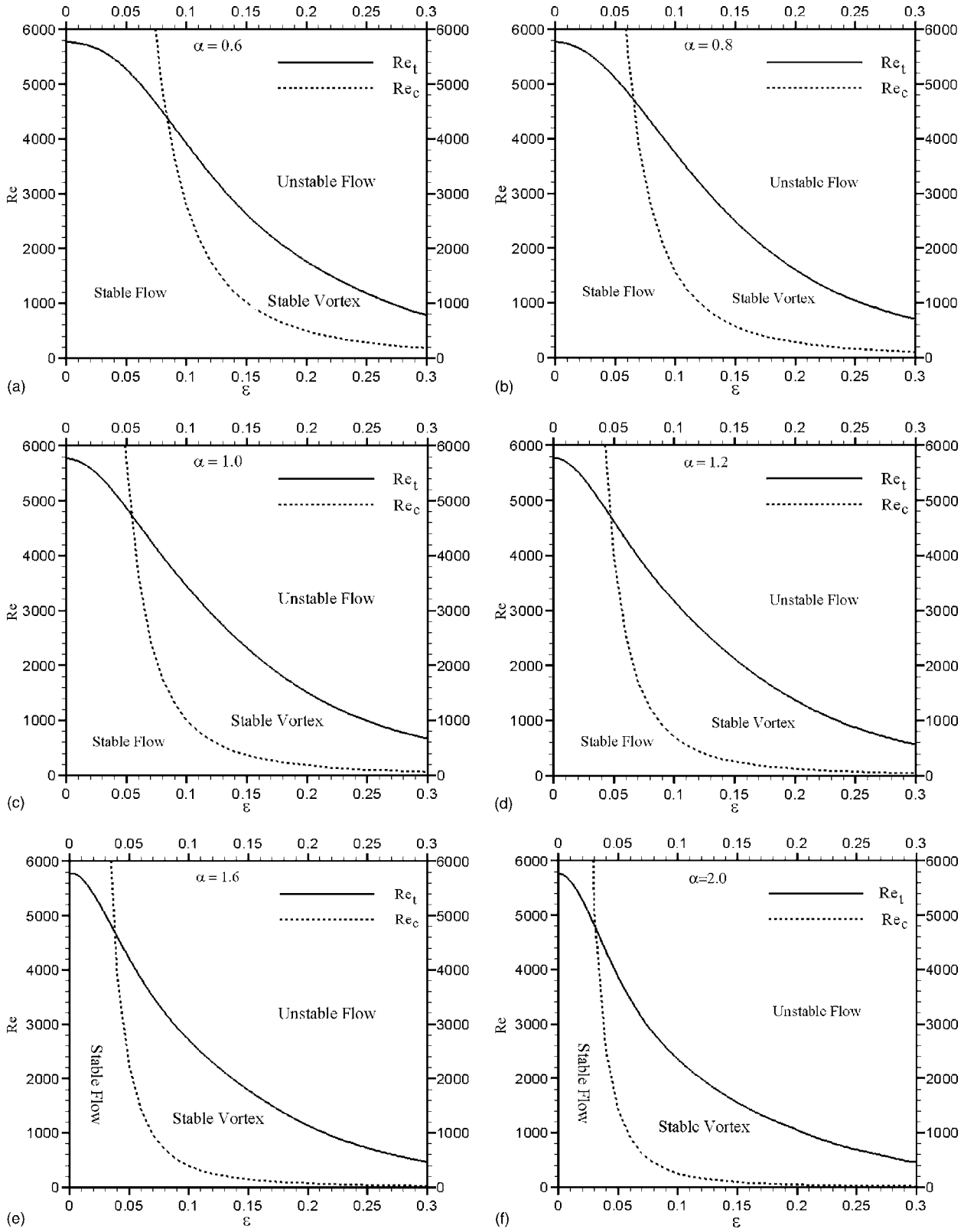

FIG. 7. Comparison between the influence of the wall modulation amplitude on the critical Reynolds number for the onset of instability, Re_t, and the critical Reynolds number for the onset of vortex flow, Re_c, for $\alpha \in [0.6, 2]$. Regions I, II, III, and IV are identified as in Fig. 6.

ods, such as the spectral method. The validity of the applied numerical approach is assessed in this study.

The channel geometry is described by two parameters, namely, the wall modulation amplitude and wave number, ε and α, respectively. The flow conditions are defined using the flow Reynolds number for a reference straight channel whose height is equal to the average height of the diverging-converging channel. A perturbation approach is applied to

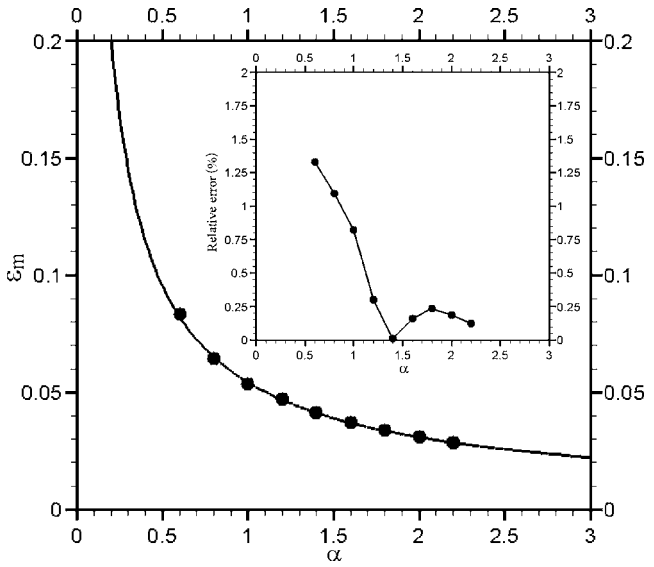

FIG. 8. Influence of the wall modulation wave number on the minimum wall modulation amplitude below which stable vortex flow cannot set in, ε_m. The solid line represents the fit from Eq. (16), and the symbols correspond to the intersections between Re_t and Re_c in Fig. 7. The inset shows the relative error for the estimation of ε_m from Eq. (16) as a function of α.

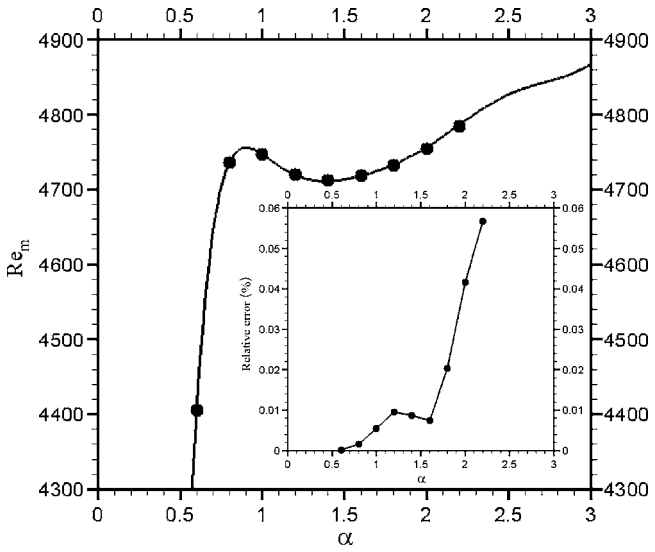

FIG. 9. Influence of the wall modulation wave number on the maximum Reynolds number above which stable vortex flow cannot set in, Re_m. The solid line represents fitting, and the symbols correspond to the intersections between Re_t and Re_c in Fig. 7. The inset shows the relative error resulting from fitting Re_m as a function of α.

calculate the steady flow through modulated channels. It is demonstrated that vortex flow in the region of expansion emerges as the Reynolds number exceeds a critical threshold Re_c. Wall corrugations influence the critical conditions for the onset of hydrodynamic instability. In particular, pressure-driven flow through modulated channel loses its stability at a critical Reynolds number Re_t lower than that for a plane (Poiseuille) channel flow.

Critical flow conditions leading to the onset of instability are demonstrated for various combinations of geometric parameters. It is found that Re_t decreases quadratically as ε increases in the small ε and α region. Vortex flow affects the conditions for the onset of instability. In fact, Re_t decreases more significantly as ε increases above the minimum wall amplitude for the onset of stable vortex flow, ε_m. Re_t is shown to decrease linearly with increasing α. Regions of stable vortex flow for various wall modulation wave numbers are demonstrated here through the comparison between Re_t and Re_c. The size of stable vortex flow regions is found to initially expand and then saturate as α increases. Explicit relations between the minimum Reynolds number for the onset of stable vortex flow, Re_m, and α, and ε_m and α are established here.

The question when Squire's theorem loses its validity is critical. However, it is outside the scope of the current work. The main objective here is to develop and implement a valid and easy numerical technique to investigate the hydrodynamic stability of the flow inside modulated channels. The developed numerical technique can be expanded to conduct a fully three-dimensional stability analysis. The influence of three-dimensional disturbances is an important issue that is worth investigating, especially since the existing literature indicates that a geometrical range exists where Squire's theorem is not valid [22]. The reported range is limited to a particular wall modulation wavelength, which is outside the valid geometrical range of the current study. Furthermore, only the upper limit of this range is reported. A universal relation to determine the critical range where three-dimensional instability sets in cannot be determined from this single reference.

Because of the accuracy and the simplicity of the developed numerical technique, it can be implemented to investigate the stability of non-Newtonian fluids inside corrugated passages in the inertial regime. Given the complexity of the geometries and the nonlinearities involved (of elastic and inertial nature), performing linear or nonlinear stability analysis using any conventional method is too stiff [6]. The interested reader is referred to the recent papers by Abu-Ramadan and Khayat [7,8] for further discussion of the flow of non-Newtonian fluids inside modulated passages.

ACKNOWLEDGMENT

The work is supported by the Natural Sciences and Engineering Research Council of Canada.

[1] I. J. Obey, J. Fluid Mech. **96**, 1 (1980).
[2] K. D. Stephanoff, I. J. Sobey, and B. J. Bellhouse, J. Fluid Mech. **96**, 27 (1980).
[3] S. Selvarajan, E. G. Tulapurkara, and V. Vasanta Ram, Phys. Fluids **11**, 579 (1999).
[4] S. Tsangaris and E. Leiter, J. Eng. Math. **18**, 89 (1984).
[5] R. C. Yalamanchili, A. Sirivat, and K. R. Rajagopal, J. Non-Newtonian Fluid Mech. **58**, 243 (1995).
[6] S. Pilitsis and A. N. Beris, J. Non-Newtonian Fluid Mech. **39**, 375 (1991).
[7] E. Abu-Ramadan and R. E. Khayat, Int. J. Numer. Methods Fluids **48**, 467 (2005).
[8] E. Abu-Ramadan and R. E. Khayat, Int. J. Numer. Methods Fluids **51**, 117 (2006).
[9] G. Leneweit and D. Auerbach, J. Fluid Mech. **387**, 129 (1999).
[10] A. Günther and P. R von Rohr, J. Fluid Mech. **478**, 257 (2003).
[11] H. Stüer, Ph.D. thesis, Swiss Federal Institute of Technology (ETH), ETH Dissertation No. 13132, 1999 (unpublished).
[12] A. Cabal, J. Szumbarski, and J. M. Floryan, J. Fluid Mech. **457**, 191 (2002).
[13] H. Zhou, R. E. Khayat, R. J. Martinuzzi, and A. G. Straatman, Int. J. Numer. Methods Fluids **39**, 1139 (2002).
[14] H. Zhou, R. J. Martinuzzi, R. E. Khayat, A. G. Straatman, and E. Abu-Ramadan, Phys. Fluids **15**, 3114 (2003).
[15] S. Selvarajan, E. G. Tulapurkara, and V. Vasanta Ram, Int. J. Numer. Methods Fluids **26**, 519 (1998).
[16] E. G. Feindt, Jahrb. 1956 Schi_bautechnischen, Ges. **50**, 180 (1956).
[17] J. M. Kendall, AIAA Pap. **81**, 195 (1981).
[18] E. Reshotko and L. Leventhal, AIAA Pap. **81**, 1224 (1981).
[19] E. Reshotko, in *Turbulent and Chaotic Phenomena*, Proceedings of IUTAM Symposium, Kyoto, Japan, edited by T. Tatsumi (North-Holland, Amsterdam, 1984).
[20] T. C. Corke, A. Bar Sever, and M. V. Morkovin, Phys. Fluids **29**, 3199 (1986).
[21] A. Kwang-Hua Chu, Phys. Rev. E **68**, 046305 (2003).
[22] F. Nicoud and J. R. Angilella, Phys. Rev. E **56**, 3000 (1997).
[23] T. Nishimura, S. Murakami, S. Arakawa, and Y. Kawamura, Int. J. Heat Mass Transfer **33**, 835 (1990).
[24] T. Nishimura, Y. Ohoriand, and Y. Kawamura, J. Chem. Eng. Jpn. **17**, 466 (1984).
[25] S. Blancher, R. Creff, and P. Le Quere, Int. J. Heat Fluid Flow **19**, 39 (1998).
[26] A. M. Guzmán and C. H. Amon, Phys. Fluids **6**, 1994 (1994).
[27] A. Lahbabi and H. C. Chang, Chem. Eng. Sci. **41**, 2487 (1986).
[28] S. A. Codington and N. Levinson, *Theory of Ordinary Differential Equations* (McGraw-Hill, New York, 1965).
[29] G. A. Ache, SIAM (Soc. Ind. Appl. Math.) J. Sci. Stat. Comput. **10**, 1097 (1989).
[30] G. A. Ache and D. Cores, J. Comput. Phys. **116**, 180 (1995).
[31] V. Pereyra, in V. Pereyra, in Lecture Notes in Computer Science Vol. 76 (Springer-Verlag, Berlin, 1978), p. 67.Lecture Notes in Computer Science Vol. 76 (Springer-Verlag, Berlin, 1978), p. 67.
[32] S. A. Orszag, J. Fluid Mech. **50**, 689 (1971).
[33] K. J. Cho, M-U. Kim, and H. D. Shin, Fluid Dyn. Res. **23**, 349 (1998).
[34] C. E. Grosch and H. Salwen, J. Fluid Mech. **34**, 177 (1968).
[35] J. Luo and X. Wu, Phys. Fluids **16**, 2858 (2004).
[36] E. L. Koshmieder, *Benard Cells and Taylor Vortices* (Cambridge University Press, New York, 1993).
[37] Abu Ramadan, Ph.D. thesis, The University of Western Ontario, London, ON, 2005 (unpublished).